Wall-Parallel PIV Measurements in Turbulent Boundary Layers with Highly Directional Surface Roughness

Kevin, B. Nugroho, J. P. Monty and N. Hutchins

Department of Mechanical Engineering
The University of Melbourne, Victoria 3010, Australia

Abstract

The potential of converging-diverging-aligned (hereafter referred to as CDA) riblets on reorganising the large-scale coherent structures that populate the logarithmic region of turbulent boundary layers is investigated at moderate Reynolds number using Particle Image Velocimetry (PIV). This work is motivated by the analysis of the pre-multiplied energy spectra of streamwise velocity fluctuations presented by Nugroho *et al.* [10], which shows an increase (or decrease) in the large-scale turbulence energy contribution over the converging (or diverging) region of the CDA riblets. The ability of CDA riblets to generate large-scale counter-rotating roll-modes [11] suggests that a preferential arrangement of the naturally occurring large-scale structures may have been introduced. In this study we examine this possible spanwise redistribution of the coherent structures using instantaneous PIV fields measured in wall-parallel (streamwise-spanwise) planes within the logarithmic region. The analysis will also briefly look at the spanwise periodicity of the region of intense vorticity.

Introduction

Conventional streamwise-aligned riblets with various cross-sectional geometries have been studied extensively due to their ability to reduce the skin-friction drag in turbulent boundary layers. Choi [3] summarised their possible drag reducing mechanisms and attribute them to the decrease in near-wall instability and a weakening of the interaction between the near-wall vortices and the wall. The highest drag reduction reported was achieved using very-thin blade cross-sections (with optimised height, spacing and thickness), giving about 9.9% reduction according to Bechert et al. [2].

Hutchins and Marusic [5] found that the large-scale structures in the logarithmic region become increasingly comparable in energy as the Reynolds number increases. These structures also have a distinct modulating influence on the small-scale energy near the wall according to Mathis *et al.* [8]. Based on this notion, a new type of riblet that can interact with these large-scale structures is proposed. Koeltzsch *et al.* found that CDA riblets are able to generate large-scale azimuthal variation in the streamwise mean velocity and turbulence intensity in a pipe flow. Nugroho *et al.* [11] mentioned that the turbulent secondary flow (in the form of large-scale counter-rotating roll-modes) generated by CDA riblets redistributes the streamwise turbulence energy. The aim of the current experiment is to instantaneously investigate how the large-scale structures behave under this deliberately imposed secondary flow.

Experimental Setup

Wind Tunnel Facility

The experiments were performed in an open-return blower wind tunnel at the University of Melbourne. The test section is 6.7 m long with cross-sectional area of 0.94×0.375 m. The roof of the wind tunnel is fully adjustable to enable accurate adjustment of the pressure gradient. The wind tunnel has a low freestream turbulence level of 0.2%. The measurements were conducted in a zero pressure gradient (ZPG) turbulent boundary layer at 4 m downstream of the tripped inlet to the test section similar to [10, 11]. All measurements presented here have a freestream velocity $U_\infty = 15$ m/s.

Converging-Diverging Riblets

The riblet surface investigated here was the same as that originally fabricated and studied by Nugroho et al. [10, 11]. Figure 1 (b) shows a schematic diagram of the CDA riblets. The surface consists of a repeating pattern of alternating converging and diverging grooves arranged in "herringbone" like fashion. The height of each rib is $h = 0.5$ mm and the spacing is $s = 0.675$ mm, giving $h^+ = hU_{\tau s}/\nu \approx 18$ and $s^+ = hU_{\tau s}/\nu \approx 24$ ($U_{\tau s}$ is the smooth-wall friction velocity at the corresponding streamwise location and freestream velocity). The riblets are yawed at an angle $\gamma = 20°$ to the mean streamwise flow direction to create regions of convergence and divergence. The width of each converging/diverging region is 73.75 mm, giving a repeating spanwise wavelength $\Lambda = 147.5$ mm ($\Lambda/\delta_s \approx 3$, where δ_s is the boundary layer thickness of the smooth-wall case at the corresponding freestream velocity). The readers are referred to [10] for full details of the riblets manufacturing technique. At the measurement location, the riblet surface was dyed black using polymeric colourant to reduce background reflection in the PIV images.

PIV Experiments

Planar PIV experiments were conducted within the logarithmic region of the turbulent boundary layer over the smooth-wall and CDA riblets at $z = 5$ mm ($z_s^+ = zU_{\tau s}/\nu \approx 180$ and $z_r^+ = zU_{\tau r}/\nu \approx 200$). The subscript '$s$' and '$r$' refer to the smooth and rough cases respectively. The friction velocity over the riblet surface $U_{\tau r}$ was estimated using modified-Clauser method, and it was taken as the spanwise-averaged value over one converging-diverging wavelength Λ. The reader are referred to [10] for further details of this estimation. The flow was seeded with polyamide particles with mean diameter of 1μm. The particles were illuminated by a 1 mm thick laser sheet generated by a Quantel EverGreen double-pulse Nd:YAG laser that delivered 200 mJ/pulse. The imaging system is a PCO4000 camera (4008×2672 pixels, 14-bit frame-straddled CCD). The camera was equipped with a Sigma 105 mm macro lens and the object distance between the camera sensor and the light sheet was approximately 500 mm. A schematic diagram of the PIV set-up is provided
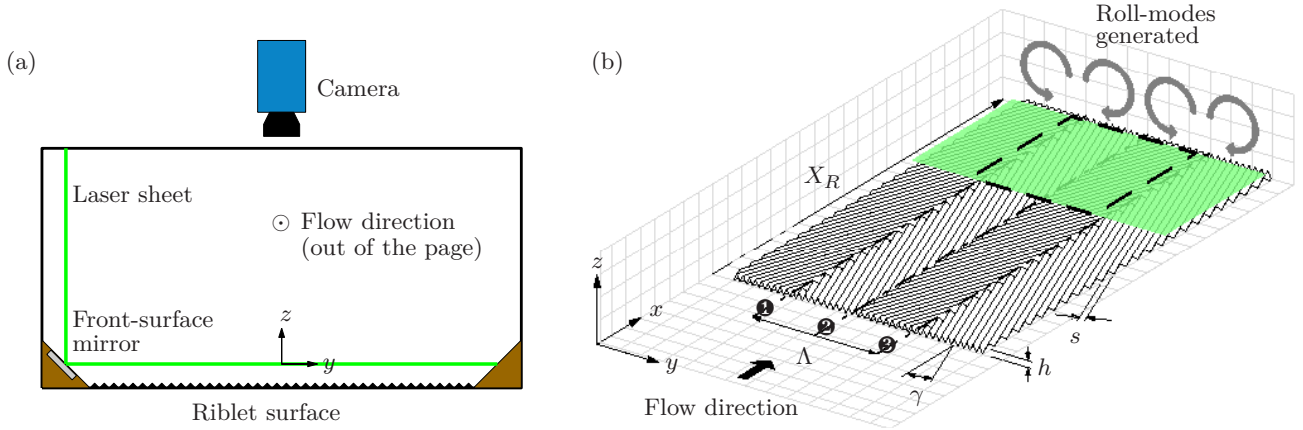
Figure 1. (a) Schematic diagram of the PIV setup showing the cross-section of the wind-tunnel working section; (b) Schematic diagram of the CDA riblets, showing the surface parameters and measurement plane. The circled numbers point out the converging (❶ & ❸) and diverging (❷) regions.

in figure 1 (a). The particle images were processed using an in-house PIV package. A final interrogation window size of 16×16 with 50% overlap was employed for both measurements, yielding a viscous-scaled interrogation volume of approximately $25 \times 25 \times 35$ for the smooth and $28 \times 28 \times 40$ for the rough surface. The details of the PIV processing algorithm are available in de Silva *et al.* [12]. Two thousand statistically independent velocity fields were acquired.

Velocity Fields

Here x, y and z correspond to the streamwise, spanwise and wall-normal direction respectively, with u, v and w denoting the respective instantaneous velocity components. To accommodate the spanwise periodicity generated by the CDA riblets, the velocity components are decomposed into three components (Coceal & Belcher [4]),

$$u_i = U_i(z) + \tilde{u}_i(x,y,z) + u_i''(x,y,z,t)$$
$$= U_i(z) + u_i'(x,y,z,t) \qquad (1)$$
$$= \overline{u}_i(x,y,z) + u_i''(x,y,z,t)$$

where U_i is the spatially and temporally averaged mean velocity (global mean), and $\tilde{u}_i = \overline{u}_i - U_i$ is the spatial variation of the time-averaged velocity. The term u_i'' is the turbulence fluctuation (convecting turbulence) about the time-averaged mean, and u_i' is the combination of both convecting and non-convecting fluctuations. Figure 2 (a) and (b) show the time-averaged streamwise $\overline{u}$ and spanwise velocity field $\overline{v}$ (normalised by the freestream velocity U_∞) in the wall-parallel plane at $z = 5$ mm above the crest of the CDA riblets. Both x and upper y-axes are normalised by the corresponding smooth-wall boundary layer thickness δ_s, with the lower y-axis normalised by the riblet wavelength Λ. Here the diverging region is located at $y/\Lambda = 0$ and converging region at $y/\Lambda = -0.5$ & 0.5. The streamwise mean velocity field for the CDA riblets exhibits a strong spanwise periodicity; the velocity over the diverging region is almost 1.5 times that above the converging region. The spanwise mean velocity field show the secondary positive and negative cross-flow generated by the riblet surface, with a diverging flow located above the diverging region of the riblets.

Figure 3 (a) and (b) show the representative instantaneous streamwise fluctuating velocity fields (normalised by their corresponding freestream velocity U_∞) over the
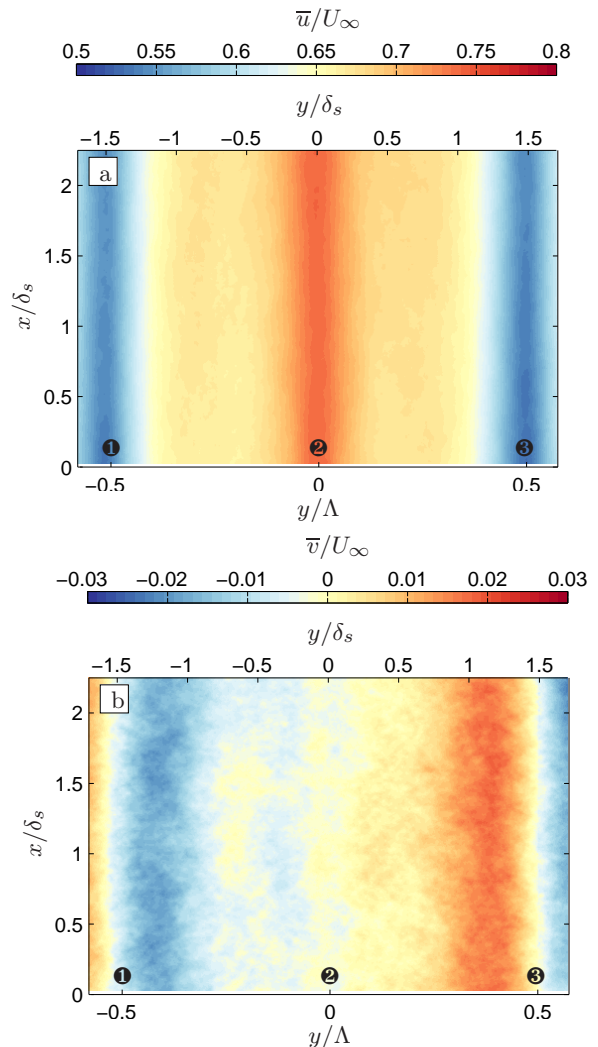

Figure 2. Time-averaged streamwise (a) and spanwise (b) velocity field (normalised by the corresponding freestream velocity U_∞) over the CDA riblets $z = 5$ mm

smooth-wall and CDA riblets, respectively. The subtraction of time and space averaged streamwise velocity U is used to highlight the riblets effect (in the mean secondary flow generated) on the fluctuating fields. Note that in the smooth-wall instance, the streamwise velocity fluctuation field is populated by δ-scale regions of positive (high
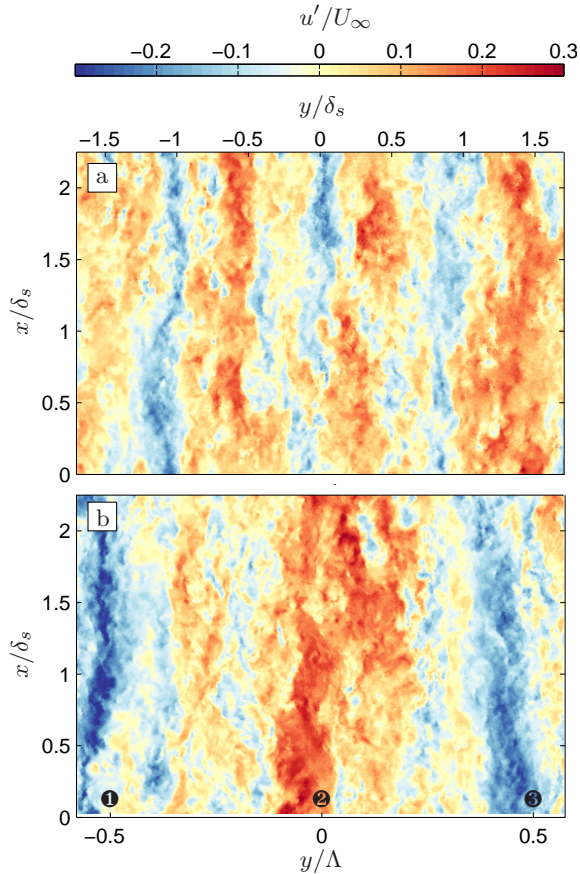
Figure 3. Representative instantaneous fluctuating velocity fields about the time and space averaged mean velocity u' normalised by their corresponding freestream value U_∞ over (a) smooth-wall and (b) CDA riblets at $z = 5$ mm.
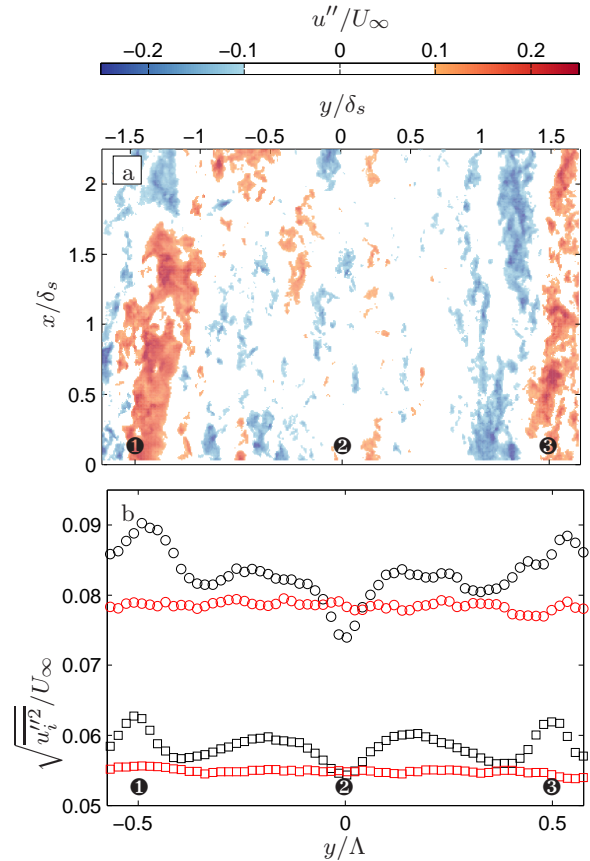

Figure 4. (a) Representative instantaneous convecting turbulence fluctuation over the CDA riblets at $z = 5$ mm. (b) Spanwise distribution of Reynolds stresses, where $\circ$ & $\square$ symbols denote streamwise and spanwise component respectively and red & black denote smooth-wall and riblet surface.

momentum region) and negative (low momentum region) fluctuations that are found to exist in the logarithmic region of turbulent boundary layers (Tomkins and Adrian [13]). These very large scale structures are also known to have significant meandering tendency and can extend up to the edge of the boundary layer (Hutchins and Marusic [6]). The instantaneous field over the riblets however, shows significant difference in the low momentum region (LMR) and high momentum region (HMR) arrangement. Strong retarded features seem to often occupy the region over the converging part of the riblet. This occurrence is interpreted as preferential pathways of the LMR. The idea of LMR's preferential pathways was mentioned previously by Mejia-Alvarez and Christensen [9] and Barros and Christensen [1] in their observation of the flow over replicated turbine blade roughness. Significant differences in the width of the structures are also apparent visually, with the wider structures occupying the diverging region (also apparent in the mean velocity field).

The large-scale counter-rotating roll-modes induced by the CDA (which are predicted to scale with the riblet wavelength Λ) seem to have gathered the low speed fluid, relocating the very large scale meandering structures over the converging part of the riblets, and hence thickening the local boundary layer. As previously shown by Nugroho *et al.*, the riblets influence will also be seen in the spanwise variation of convecting turbulence fluctuation u'' (which is a fluctuation about the local time-averaged mean). Figure 4(a) shows the representative instantaneous streamwise turbulence fluctuation u'' (normalised by the corresponding freestream velocity U_∞) of the current study. A

threshold is applied on the colour plot only to show the region of $|u''|/U_\infty > 0.1$. Notice that the region over the converging part of CDA riblets are often inhabited by large positive and negative turbulence fluctuations (with nominally zero skewness similar to the log region of smooth-wall boundary layers), while much weaker fluctuations are observed over the diverging region. Figure 4(b) shows the standard deviation distribution of the streamwise ($\circ$) and spanwise ($\square$) velocity component, over the smooth-wall (red symbols) and CDA riblets (black symbols). Both components of Reynolds stresses over the CDA riblets seem to be higher at this wall location (except for the small region around the diverging part). This behaviour (of the streamwise component) is consistent with previous study by Nugroho *et al.* [10, 11].

Wall Normal Vorticity

Figure 5(a) shows a representative instantaneous wall-normal vorticity normalised by the freestream velocity $\omega_z = (\frac{du}{dy} - \frac{dv}{dx})\nu/U_\infty^2$. A threshold is again applied on the contour plot to show only regions of intense positive or negative vorticity. The grey background colour is the corresponding u'. It can be seen that the large scale low momentum structures are flanked by high vorticity features, which is consistent with the presence of hairpins/packets. Figure 5(b) shows the time-averaged of wall-normal vorticity fluctuation squared (calculated based on the convecting turbulence fluctuation) normalised by the freestream velocity $\overline{\omega_z''^2} = \overline{(\frac{du''}{dy} - \frac{dv''}{dx})^2}\nu/U_\infty^2$. The figure
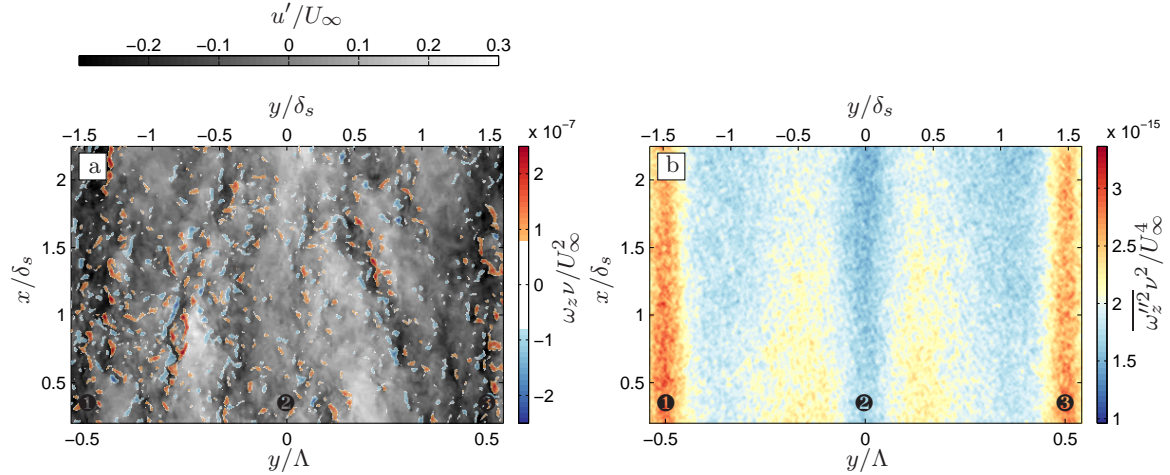
Figure 5. (a) Representative instantaneous wall-normal vorticity field (normalised by the freestream velocity) over the CDA riblets, with grey background of the corresponding streamwise velocity fluctuations. (b) Time-averaged wall-normal vorticity fluctuation squared (normalised by the freestream velocity)

clearly shows that the strength of vortical activity is not distributed evenly over the CDA riblets. Regions over the converging section are populated with more intense features, while lower vorticity features are observed over the diverging section. Isolating the vorticity from the mean velocity gradient indicates that features with high with vortical activity indeed have preferential pathways over the converging part of the riblets.

Conclusion

A study has been conducted in the logarithmic region of ZPG turbulent boundary layers to examine the flow modifications caused by CDA riblets. The instantaneous streamwise velocity fluctuation field (about the global mean) reveals clear preferential pathways for the LMR and HMR for the same physical height above the riblet surface. A noticeable difference in the width of the large-scale structures is also observed. An increase in the streamwise and spanwise components (normalised with freestream velocity) of the Reynolds stress is observed, except in the region close to the diverging part of the CDA riblets. Spanwise inhomogeneity of the wall-normal vorticity based on the convecting turbulence fluctuation is also observed, where the region over the converging sections of the riblets become the preferential pathways of vortical features.

Acknowledgements

References

[1] Barros, J. M., Christensen, K. T., Observations of turbulent secondary flows in a rough-wall boundary layer, *J. Fluid Mech.*, **748**, 2014, R1

[2] Bechert, D. W., Bruse, M., Hage, W., van der Hoeven, J. G. T. and Hoppe, G., Experiments on drag-reducing surfaces and their optimization with an adjustable geometry, *J. Fluid Mech.*, **338**, 1997, 59-87

[3] Choi, K. S., Near-wall structure of a turbulent boundary layer with riblets, *J. Fluid Mech.*, **208**, 1989, 417-458

[4] Coceal, O. and Belcher, S. E., A canopy model of mean winds through urban areas. *Quart. J. R. Met. Soc.*, **130**, 2004, 1349-1372.

[5] Hutchins, N. and Marusic, I., Large-scale influences in near-wall turbulence. *Phil. Trans. R. Soc. A*, **365**, 2007, 647-664

[6] Hutchins, N. and Marusic, I., Evidence of very long meandering features in the logarithmic region of turbulent boundary layers, *J. Fluid Mech.*, **579**, 2007, 1-28

[7] Koeltzsch, K., Dinkelacker, A., Grundmann, R., Flow over convergent and divergent wall riblets, *Exp. Fluids*, **33**, 2002, 346-350

[8] Mathis, R., Hutchins, N., Marusic, I., Large-scale amplitude modulation of the small-scale structures in turbulent boundary layers, *J. Fluid Mech.*, **628**, 2009, 311

[9] Mejia-Alvarez, R., Christensen, K. T., Wall-parallel stereo particle-image velocimetry measurements in the roughness sublayer of turbulent flow overlying highly irregular roughness , *Phys. Fluids*, **25**, 2013, 115109

[10] Nugroho, B. and Hutchins, N. and Monty, J. P., Large-scale spanwise periodicity in a turbulent boundary layer induced by highly ordered and directional surface roughness. *Int. J. Heat Fluid Flow*, 41:90-102, 2013

[11] Nugroho, B. and Gnanamanickam, E. P. and Kevin and Monty, J. P. and Hutchins, N., Roll-modes generated in turbulent boundary layers with passive surface modifications. *AIAA*, 52, 2014

[12] de Silva, C. M., Gnanamanickam, E. P., Atkinson, C., Buchman, N. A., Hutchins, N., Soria, J., Marusic, I., High spatial range velocity measurements in a high Reynolds number turbulent boundary layers, *Phys. of Fluids*, **26**, 2014, 025117

[13] Tomkins, C. D., Adrian, R. J., Spanwise structure and scale growth in turbulent boundary layers, *J. Fluid Mech.*, **490**, 2003, 37-74